Geophysical Detection of Relict Metasomatism from an Archean (~3.5 Ga) Subduction Zone

Chin-Wu Chen, *et al.*

Science **326**, 1089 (2009);
DOI: 10.1126/science.1178477

15. J. Farquhar, B. A. Wing, in *Mineral Deposits and Earth Evolution*, I. McDonald, A. J. Boyce, I. B. Butler, R. J. Herrington, D. A. Polya, Eds. (Geological Society of London Special Publication, London, 2005), vol. 248, pp. 167–177.
16. Y. Ueno, S. Ono, D. Rumble, S. Maruyama, *Geochim. Cosmochim. Acta* **72**, 5675 (2008).
17. H. Bao, D. Rumble III, D. R. Lowe, *Geochim. Cosmochim. Acta* **71**, 4868 (2007).
18. J. W. Jamieson, B. A. Wing, M. D. Hannington, J. Farquhar, *Econ. Geol.* **101**, 1055 (2006).
19. S. Ono, N. J. Beukes, D. Rumble III, *Precambrian Res.* **169**, 48 (2009).
20. Y. Shen, J. Farquhar, A. Masterson, A. J. Kaufman, R. Buick, *Earth Planet. Sci. Lett.* **279**, 383 (2009).
21. P. Philippot *et al.*, *Science* **317**, 1534 (2007).
22. O. Rouxel, A. Bekker, K. Edwards, *Science* **307**, 1088 (2005).
23. B. L. Beard *et al.*, *Chem. Geol.* **195**, 87 (2003).
24. Supporting material is available on *Science* Online.
25. O. Rouxel, W. C. Shank III, W. Bach, K. J. Edwards, *Chem. Geol.* **252**, 214 (2008).
26. J. A. Schuessler, R. Schoenberg, H. Behrens, F. Von Blanckenburg, *Geochim. Cosmochim. Acta* **71**, 417 (2007).
27. F.-Z. Teng, N. Dauphas, R. T. Helz, *Nature* **320**, 1620 (2008).
28. C. M. Johnson, B. L. Beard, N. J. Beukes, C. Klein, J. M. O'Leary, *Contrib. Mineral. Petrol.* **144**, 523 (2003).
29. J. G. Foster, D. D. Lambert, L. R. Frick, R. Mass, *Nature* **382**, 703 (1996).
30. C. M. Lesher, M. O. Burnham, *Can. Mineral.* **39**, 421 (2001).
31. M. E. Barley, A. Bekker, B. Krapez, *Earth Planet. Sci. Lett.* **238**, 156 (2005).
32. N. M. Rosengren, S. W. Beresford, B. A. Grguric, R. A. F. Cas, *Econ. Geol.* **100**, 149 (2005).
33. M. D. Hannington, W. Bleeker, I. Kjarsgaard, in *The Giant Kidd Creek Volcanogenic Massive Sulfide Deposit, Western Abitibi Subprovince, Canada*, M. D. Hannington, C. Tucker Barrie, Eds. (Economic Geology, Monograph 10, 1999), pp. 163–224.
34. Supported by a NAI International Collaboration grant (M.L.F.); AMIRA and the Australian Research Council DP 0988326 grants (M.E.B., M.L.F., and S.W.B.); NSF grant EAR-937 05-45484 (A.B.); NAI award NNA04CC09A (A.B.); Natural Sciences and Engineering Research Council of Canada 938 Discovery grant (A.B.); NAI, Carnegie Institution of Washington Node, and NASA Cosmochemistry program (D.R.); and NSF OCE-0622982 and EAR-0820661 grants (O.J.R.). We acknowledge R. Cas, M. Houlé, M. Lesher, J. Farquhar, A. L. Masterson, and M. Auro for helpful discussions and experimental assistance and two anonymous reviewers for constructive comments.

Supporting Online Material

www.sciencemag.org/cgi/content/full/326/5956/1086/DC1
Materials and methods
SOM Text
Figs. S1 to S4
Table 1
References

15 June 2009; accepted 14 September 2009
10.1126/science.1177742

Geophysical Detection of Relict Metasomatism from an Archean (~3.5 Ga) Subduction Zone

Chin-Wu Chen,[1]* Stéphane Rondenay,[1] Rob. L. Evans,[2] David B. Snyder[3]

When plate tectonics started on Earth has been uncertain, and its role in the assembly of early continents is not well understood. By synthesizing coincident seismic and electrical profiles, we show that subduction processes formed the Archean Slave craton in Canada. The spatial overlap between a seismic discontinuity and a conductive anomaly at ~100 kilometers depth, in conjunction with the occurrence of mantle xenoliths rich in secondary minerals representative of a metasomatic front, supports cratonic assembly by subduction and accretion of lithospheric fragments. Although evidence of cratonic assembly is rarely preserved, these results suggest that plate tectonics was operating as early as Paleoarchean times, ~3.5 billion years ago (Ga).

Archean cratons form the core of many of Earth's continents. By virtue of their longevity, they offer important clues about plate tectonic processes during early geological times. A question of particular interest is whether subduction is the main mechanism of cratonic assembly and, if so, when this process began to operate. Answers to these questions may be found in the lithosphere of the Archean Slave craton, which is located in the northwestern Canadian Shield (Fig. 1) and represents the oldest known fragment of the North American continent (*1*). The Slave craton has been studied extensively to reveal processes of cratonic assembly as it is well exposed and has been insulated from plate margin processes for more than 2 billion years. In the center of the Slave craton, inclusions of rock fragments from the mantle indicate that the lithospheric mantle is separated into two distinct layers at 140- to 150-km depth, with a harzburgitic upper layer exhibiting a very high degree of iron depletion (*2*, *3*) and a lherzolitic lower layer that is less depleted in iron (*2*). Previous seismic studies identified remnants of subducted oceanic lithosphere (*4*–*6*), believed to be linked to the final stages of assembly of the Slave craton during the late Archean (~2.6 Ga) and to its stabilization during the Proterozoic (~1.84 Ga). Despite these results, there remains much uncertainty over the timing and mechanisms of the formation of the Slave craton. For example, it is unknown when its >200-km-thick lithospheric root was in place, and if it was constructed solely by subduction accretion (*7*) or by successive accretion-collision episodes (*8*).

Here, we investigate coincident seismic receiver-function (*9*) and electrical profiles across the Slave craton to further understand the mechanisms of cratonic assembly. Two main features in the seismic profile reveal the structure of the underlying lithosphere (Fig. 2). First, the crust-mantle boundary, or Moho, appears as a positive (downward slow-to-fast) velocity gradient across the entire profile at depths ranging from 34 to 41 km, marking a southward thickening of the crust. Second, a pronounced negative (downward fast-to-slow) velocity gradient dips southward from 96- to 124-km depth beneath the center of the craton. Portions of this seismic discontinuity have been identified previously (*5*, *6*), but here it is seen as a continuous profile. The lack of *SH*-response by the seismic discontinuity (*9*) suggests that it is not caused by anisotropic parameters (*4*). Thus, the amplitude of the discontinuity suggests a 9 to 21% isotropic velocity contrast (*9*).

The electrical image was constructed by means of the magnetotelluric (MT) technique, which measures time variations of the magnetic and electric fields at Earth's surface to infer electrical resistivity structure in the subsurface, and reveals a conductive anomaly in the central Slave mantle (*10*) (Fig. 2B). The anomaly has a conductivity of 0.01 to 0.03 S/m, which is two orders of magnitude higher than that of the surrounding mantle and therefore prevents penetration of the signal (and imaging) at greater depths. It has a depth ranging from ~80 to 120 km with a southward dip, and may be caused by interconnected graphite films deposited along grain boundaries (*10*).

When displayed simultaneously in vertical cross section (Fig. 2, A and B), the seismic discontinuity and the conductive anomaly exhibit a pronounced spatial coincidence. Although the conductive anomaly appears slightly shallower (by ~4 to 9 km) than the seismic discontinuity, this difference is within reasonable error of the depth estimates associated with each technique—namely, 10 km for the seismic profile and 15 km for the MT image (*9*, *10*). In map projection, the regions over which these structures are observed overlap with the lateral extent of the upper-mantle harzburgitic layer (*2*) (Fig. 1).

The coexistence of the seismic and electrical discontinuities suggests that they have a common origin. A review of the possible causes for these anomalies, with support from petrological analy-

[1]Department of Earth, Atmospheric, and Planetary Sciences, Massachusetts Institute of Technology (MIT), 77 Massachusetts Avenue, Cambridge, MA 02139, USA. [2]Department of Geology and Geophysics, Woods Hole Oceanographic Institution, MS 22, Woods Hole, MA 02543, USA. [3]Geological Survey of Canada, 615 Booth Street, Ottawa, Ontario K1A 0E9, Canada.

*To whom correspondence should be addressed. E-mail: cwchen@mit.edu

ses of xenoliths, favors a mineralogical explanation (*9*). A positive thermal anomaly, a layer of partial melt, or the presence of water could all lower seismic velocities (*9*), but they cannot be sustained over long time scales (millions of years) in the cold, stable lithosphere of the Slave craton. Similarly, compositional variations due to the juxtaposition of different mantle domains or to variable degrees of melt depletion cannot account for more than 1.5% of seismic velocity variation (*11*) or one-third of an order of magnitude reduction in electrical resistivity (*12*). Although no single mineral can produce both anomalies, secondary minerals that formed from metasomatic alteration may be responsible. For the seismic anomaly, phlogopite is the most likely candidate, as it is stable at pressure and temperature conditions corresponding to the location of the anomaly (*13*) and represents up to ~50% of the bulk composition of the eclogitic mantle xenoliths that originated ~100 km below the central Slave craton (*14*). This quantity of phlogopite could reduce *S*-wave velocities by ~17% relative to the host eclogite and surrounding mantle peridotite (*15*), which is in agreement with the observed seismic discontinuity. Phlogopite also increases electrical conductivity (*13*), but experimental data show that it can contribute at most 1% of the observed conductive anomaly (*16*). We attribute the additional conductivity increase to thin, interconnected films of graphite deposited along grain boundaries, the presence of which has been invoked to explain this and other conductivity anomalies in cratonic lithosphere (*10*, *17*).

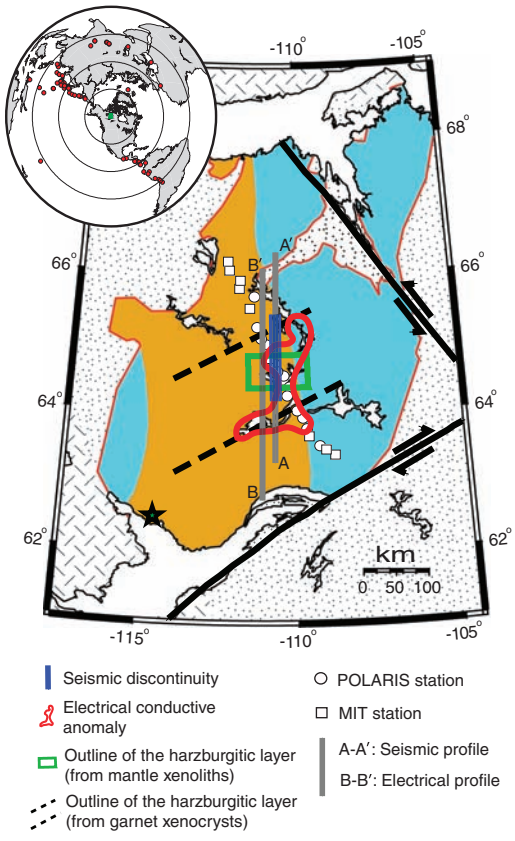

Fig. 1. Map of the Slave craton. The boundaries of the exposed craton are outlined in red. Inset shows a polar projection of the world centered on the craton (green square), with the 62 earthquakes (red circles) used for the analysis. Crustal topology and geochemical signatures broadly subdivide the Slave craton into two distinct regions (*27*): the older (4.03 to 2.83 Ga) Central Slave Basement Complex to the west, filled in brown, and isotopically juvenile rocks (2.67 to 2.6 Ga) to the east, filled in blue. The lateral extent of an ultradepleted harzburgitic layer of the mantle lithosphere has been inferred from petrological analysis of mantle xenoliths (*2*) (outlined in green) and geochemical analyses of garnet xenocrysts (*3*) (region between the two black dashed lines). The seismic stations used in this study are denoted by white circles and squares for POLARIS and MIT stations, respectively, which form a ~400-km-long linear array with ~20-km average station spacing. The line A-A′ marks the location of the seismic profile shown in Fig. 2A. The lateral extent of the central Slave seismic discontinuity (Fig. 2, A and C) is indicated by blue shading, and that of the conductive anomaly (Fig. 2B) is outlined in red. The line B-B′ is the nominal projected location of the MT array (*10*).

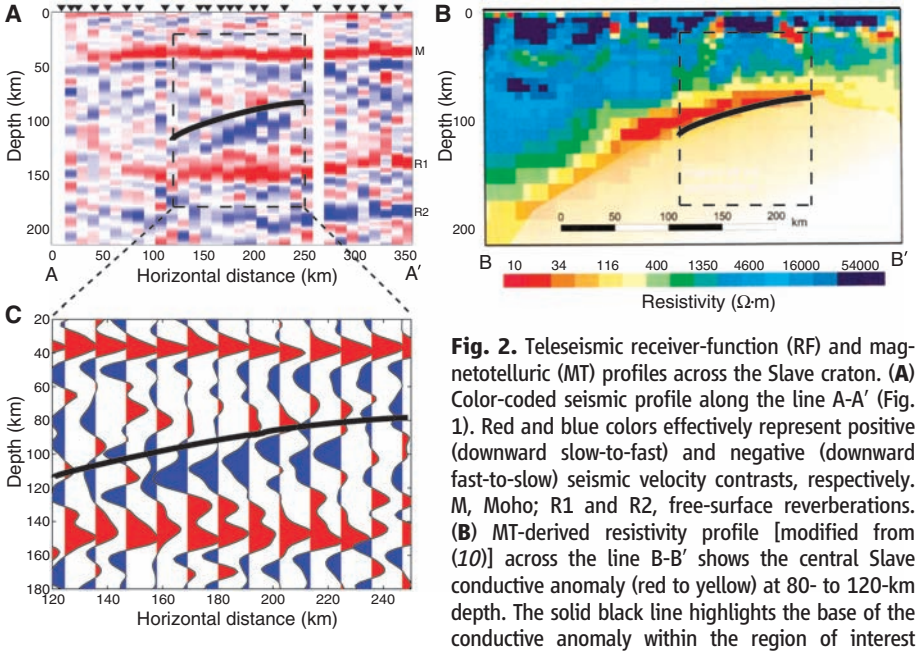

Fig. 2. Teleseismic receiver-function (RF) and magnetotelluric (MT) profiles across the Slave craton. (**A**) Color-coded seismic profile along the line A-A′ (Fig. 1). Red and blue colors effectively represent positive (downward slow-to-fast) and negative (downward fast-to-slow) seismic velocity contrasts, respectively. M, Moho; R1 and R2, free-surface reverberations. (**B**) MT-derived resistivity profile [modified from (*10*)] across the line B-B′ shows the central Slave conductive anomaly (red to yellow) at 80- to 120-km depth. The solid black line highlights the base of the conductive anomaly within the region of interest (dashed black box), repeated to scale in RF profiles for comparison. (**C**) Close-up RF traces for bins in the region of interest (*9*).

The subduction event may be constrained by the age of minerals found in local xenoliths and by the lateral extent of the observed discontinuity. Lu-Hf dating of clinopyroxenes in the phlogopite-bearing eclogites indicates a minimum age of ~2.7 Ga (*14*), which approaches closely the timing of collision between the younger eastern Slave terranes and the older Central Slave Basement Complex (Fig. 1) (*21*). However, this event caused a north-south suture that runs nearly parallel to the seismic line (*21*), and a related subduction should therefore be observed over the entire length of the profile, which is not

the case. Moreover, robust Re-Os age constraints on peridotitic diamonds from the harzburgitic layer suggest that the central Slave's lithospheric mantle down to 150 km was formed and stabilized by 3.5 Ga (*22*). Therefore, the central Slave seismic discontinuity is likely caused by metasomatized mantle from a Paleoarchean subduction zone.

The presence of a Paleoarchean cratonic lithosphere in the Slave does not conflict with the occurrence of craton-wide arc volcanism and plutonism during later Neoarchean time (*21*); rather, it suggests that the blocks that aggregated in the final stage of cratonic assembly may themselves have been fragments of older, thick proto-cratonic entities. This is consistent with the limited lateral extent of the discontinuity, which may mark the outline of a broken block (fig. S4), and is supported by the unique geochemical signature and high concentration of diamondiferous kimberlites found in the same region (*2*).

If subduction has been active since the Paleoarchean, similar or related structures with limited lateral extent should be expected in other parts of the craton and in other cratons worldwide. Indeed, anisotropic seismic discontinuities have been detected below the southwest edge of the Slave craton (*4*) and the adjacent Wopmay orogen (*23*). These have been inferred to mark Proterozoic collision-subduction events associated with the final assembly and stabilization of a large part of the Laurentian continent (*24*). Away from cratonic edges, similar seismic discontinuities have been detected in the Kaapvaal craton of South Africa (*25*). Moreover, a global compilation of long-aperture seismic refraction data indicates the existence of a widespread (albeit not ubiquitous) negative discontinuity in the 90- to 120-km depth range beneath several Archean cratons (*26*). The character of the discontinuities (i.e., their spatial extent, depth, dip, and physical properties) depends on the details of each subduction event, including the amount of metasomatism, the subduction geometry, and history of much younger events of accretion and magmatism. Given the limited detailed geophysical sampling of cratons and the nonuniform nature of these subduction-related discontinuities, it is thus not surprising that not many of them have been observed to date.

References and Notes

1. S. A. Bowring, I. S. Williams, W. Compston, *Geology* **17**, 971 (1989).
2. W. L. Griffin *et al.*, *J. Petrol.* **40**, 705 (1999).
3. H. S. Grütter, D. B. Apter, J. Kong, in *Proceedings of the 7th International Kimberlite Conference*, J. J. Gurney *et al.*, Eds. (Red Roof Design, Cape Town, 1999), vol. 1, pp. 307–313.
4. M. G. Bostock, *J. Geophys. Res.* **103**, 21183 (1998).
5. D. B. Snyder, *Tectonics* **27**, TC4006 (2008).
6. M. Moorkamp, A. G. Jones, D. W. Eaton, *Geophys. Res. Lett.* **34**, L16311 (2007).
7. H. H. Helmstaedt, J. D. Schulze, in *Kimberlites and Related Rocks, Their Composition, Occurrence, Origin, and Emplacement*, J. Ross, Ed. (Geological Society of Australia, Canberra, 1989), vol. 1, pp. 358–368.
8. T. H. Jordan, *Nature* **274**, 544 (1978).
9. Supporting material is available on *Science* Online.
10. A. G. Jones *et al.*, *Geology* **29**, 423 (2001).
11. C.-T. A. Lee, *J. Geophys. Res.* **108**, 2441 (2003).
12. A. G. Jones, R. L. Evans, D. W. Eaton, *Lithos* **109**, 131 (2009).
13. D. E. Boerner *et al.*, *Science* **283**, 668 (1999).
14. S. Aulbach, N. J. Pearson, S. Y. O'Reilly, B. J. Doyle, *J. Petrol.* **48**, 1843 (2007).
15. B. R. Hacker *et al.*, *J. Petrol.* **46**, 1661 (2005).
16. A. A. Guseinov, I. O. Gargatsev, R. U. Gabitova, *Izv. Phys. Solid Earth* **41**, 670 (2005).
17. M. Mareschal, W. S. Fyfe, J. Percival, T. Chan, *Nature* **357**, 674 (1992).
18. D. M. Kerrick, J. A. D. Connolly, *Nature* **411**, 293 (2001).
19. C.-T. A. Lee, in *Archean Geodynamics and Environments*, K. Benn, J.-C. Mareschal, K. C. Condie, Eds. (American Geophysical Union, Washington, DC, 2006), vol. 164, pp. 89–114.
20. L. S. Wagner, S. Beck, G. Zandt, M. N. Ducea, *Earth Planet. Sci. Lett.* **245**, 289 (2006).
21. W. J. Davis, A. G. Jones, W. Bleeker, H. Grütter, *Lithos* **71**, 575 (2003).
22. K. J. Westerlund *et al.*, *Contrib. Mineral. Petrol.* **152**, 275 (2006).
23. J.-P. Mercier *et al.*, *J. Geophys. Res.* **113**, B04308 (2008).
24. P. F. Hoffman, *Annu. Rev. Earth Planet. Sci.* **16**, 543 (1988).
25. D. B. Snyder, S. Rondenay, M. G. Bostock, G. D. Lockhart, *Lithos* **77**, 859 (2004).
26. H. Thybo, E. Perchuć, *Science* **275**, 1626 (1997).
27. W. Bleeker, L. Ketchum, V. Jackson, M. Villeneuve, *Can. J. Earth Sci.* **36**, 1083 (1999).

28. We thank S. Bowring for thoughtful and insightful comments on earlier drafts of this paper. We thank A. Jones for permission to use his figure in Fig. 2B. We thank S. Shirey, S. Aulbach, C. Till, L. Elkins-Tanton, and M. Moorkamp for helpful discussions, the POLARIS consortium for making data available, and members in the Northwest Territories Geoscience Office, BHP-Billiton Diamonds Inc., De Beers Canada Inc., and Tahera Diamond Corp. for logistical support of our field work in the Slave province. This work is funded by NSF grant EAR-0409509 (S.R.). C.-W.C. is partially supported by an MIT Praecis Presidential Fellowship. This is Natural Resources Canada Earth Sciences Sector (ESS) contribution 20090244.

Supporting Online Material

www.sciencemag.org/cgi/content/full/326/5956/1089/DC1
SOM Text
Figs. S1 to S4
Table S1
References

30 June 2009; accepted 17 September 2009
10.1126/science.1178477

Nanoplasmonic Probes of Catalytic Reactions

Elin M. Larsson,* Christoph Langhammer, Igor Zorić, Bengt Kasemo

Optical probes of heterogeneous catalytic reactions can be valuable tools for optimization and process control because they can operate under realistic conditions, but often probes lack sensitivity. We have developed a plasmonic sensing method for such reactions based on arrays of nanofabricated gold disks, covered by a thin (~10 nanometer) coating (catalyst support) on which the catalyst nanoparticles are deposited. The sensing particles monitor changes in surface coverage of reactants during catalytic reaction through peak shifts in the optical extinction spectrum. Sensitivities to below 10^{-3} monolayers are estimated. The capacity of the method is demonstrated for three catalytic reactions, CO and H_2 oxidation on Pt, and NO_x conversion to N_2 on Pt/BaO.

In heterogeneous catalysis, reactants in gas or liquid phase are converted to desired product molecules on the surface of a solid catalyst, which is usually composed of catalytically active nanoparticles (1 to 10 nm) dispersed on a porous, high-surface-area support material. In order to understand and improve these systems, it is important to be able to monitor the catalyst's state and to follow the reaction in real time. An important quantity is the surface coverage of reactants. However, experimental difficulties arise from the complexity of the catalyst and the atmospheric or higher pressures in which the reactions occur. Model systems (commonly single-crystal surfaces) and model reactions are frequently investigated at idealized ultrahigh vacuum (UHV) conditions, allowing use of powerful experimental probes (such as electrons, photons, or ions). A major challenge is to correlate results obtained by using the idealized and thoroughly scrutinized model catalysts in UHV with those of the less characterized real nanostructured catalysts at real reaction conditions (*1*–*3*).

We describe a method that, with a simple optical transmission (or reflection) measurement (Fig. 1A), can follow catalytic reactions in real time for both model and real supported catalysts. The principle is "nanoplasmonic" [localized surface plasmon resonance (LSPR)] sensing, currently intensely explored for biosensing, down toward single-molecule sensitivity (*4*). We show that LSPR can monitor changes in adsorbate coverages on "realistic" supported catalysts (Fig. 2) with a sensitivity corresponding to much less than 0.1 monolayer (ML).

For demonstrators, we used two types of Pt catalysts (Fig. 1, B to G) and three well-known catalytic reactions: oxidation of hydrogen ($H_2 + 1/2O_2 \rightarrow H_2O$), oxidation of carbon monoxide ($CO + 1/2O_2 \rightarrow CO_2$), and NO_x storage and

Chemical Physics Group, Department of Applied Physics, Chalmers University of Technology, SE-41296 Gothenburg, Sweden.

*To whom correspondence should be addressed. E-mail: elarsson@chalmers.se